

# Modeling tunnel profile in the presence of coordinate errors: A Gaussian process-based approach

Chen Zhang, Yong Lei, Linmiao Zhang &amp; Nan Chen


**To cite this article:** Chen Zhang, Yong Lei, Linmiao Zhang & Nan Chen (2017) Modeling tunnel profile in the presence of coordinate errors: A Gaussian process-based approach, IISE Transactions, 49:11, 1065-1077. DOI: 10.1080/24725854.2017.1348646

To link to this article: <https://doi.org/10.1080/24725854.2017.1348646>



Published online: 06 Sep 2017.



Submit your article to this journal 



Article views: 253

[View related articles](#) View Crossmark data 

Citing articles: 2 View citing articles 



# Modeling tunnel profile in the presence of coordinate errors: A Gaussian process-based approach

Chen Zhang<sup>a</sup>, Yong Lei<sup>b</sup>, Linmiao Zhang<sup>b,c</sup> and Nan Chen<sup>a</sup>

<sup>a</sup>Department of Industrial Systems Engineering and Management, National University of Singapore, Singapore; <sup>b</sup>State Key Laboratory of Fluid Power and Mechatronics Systems, Zhejiang University, Hangzhou, P.R. China; <sup>c</sup>Fab 10 Data Science, Micron Technology, Singapore

## ABSTRACT

This article presents a Gaussian process (GP)-based approach to model a tunnel's inner surface profile with high frequency sensing data provided by a Terrestrial Laser Scanner (TLS). We introduce a reading-surface profile that uniquely determines a three-dimensional tunnel in a Cartesian coordinate system. This reading-surface transforms the cylindrical tunnel to a two-dimensional surface profile, hence allowing us to model the tunnel profile by GP. To account for coordinate errors induced by TLS, we take repeated measurements at designed coordinates. We apply a Taylor approximation to extract mean and gradient estimations from the repeated measurements and then fit the GP model with both estimations to obtain a more robust reconstruction of the tunnel profile. We validate our method through numerical examples. The simulation results show that with the help of derivative estimations, our method outperforms the conventional GP regression with noisy observations in terms of mean-squared prediction error. We also present a case study to demonstrate that our method provides a more accurate result than the existing cylinder-fitting approach and has great potential for deformation monitoring in the presence of coordinate errors.

## ARTICLE HISTORY

Received 3 December 2015  
Accepted 15 June 2017

## KEYWORDS

Tunnel profile; surface reconstruction; Gaussian process; coordinates transformation; coordinate errors; gradient estimation

## 1. Introduction

Tunnel deformation is a major safety concern in underground construction projects. Minor tunnel deformations can cause shrinkage of the tunnel geometry. The shrinkage in its early stage is usually so gradual that only very small, almost unobservable, changes occur to the smooth surface of a tunnel. However, once it becomes more severe and abrupt, it can cause catastrophic rockfalls, endangering any workers inside the tunnel. Therefore, detecting tunnel deformations as early as possible is critical throughout the lifetime of a tunnel, especially during the construction period. This is the motivation of our research. To have accurate monitoring and efficient detection, we need first to have precise modeling for the tunnel profile; which is the focus of this article.

Recently, the Terrestrial Laser Scanner (TLS) technique has been applied to measure a tunnel's profile; see Monserrat and Crosetto (2008); Fekete *et al.* (2010); Han *et al.* (2013) for examples. The TLS technique is able to provide large-scale, high-resolution measurements in a short amount of time. In contrast with conventional point survey approaches, the TLS method can fully characterize the entire tunnel surface by providing three-dimensional point cloud data. To filter out measurement noise and fully utilize the point cloud data provided by the TLS method, computational approaches, such as cylinder-fitting (Van Gosliga *et al.*, 2006) or elliptical-fitting (Walton *et al.*, 2014), have been introduced to reconstruct the tunnel as a continuous surface profile. Based on the fitted model, subsequent statistical analysis (Van Gosliga *et al.* 2006) or sensitivity tests (Delaloye *et al.*, 2015) for deformation detection can be conducted.

Despite the significance of filtering the measurement noise, current cylindrical-fitting approaches have some limitations. In practice, the tunnel surfaces are barely in perfect cylindrical geometry. For instance, Figure 1 shows a piece of tunnel segment and the corresponding cylinder model fitted using point cloud measurements. As we can observe from Figure 1(a), the tunnel surface can be rather complex, and from Figure 1(b) the parametric cylinder model lacks sufficient flexibility to capture local variations in the surface. Unfortunately, as this local variability contains information about minor deformations, these methods will fail to detect these deformations in the early stage. In this regard, a more flexible and accurate model is preferable. Moreover, tunnel profiles usually have spatial correlations, which are caused by the similar process conditions of adjacent points. For example, in the formwork removal of the lining process, the spatial correlations of the formwork profiles create spatial correlations in the tunnel profiles. Actually, in addition to these spatial correlations introduced by construction, a nonuniform rock density naturally leads adjacent places to experience similar conditions and be spatially correlated (Li *et al.*, 2011). As a result, it is important to account for the spatial structure to improve the accuracy of a model.

Considering the challenges and features of modeling a tunnel's profile, the Gaussian Process (GP) is a promising model. First, it has been used to model complex profiles in a wide range of applications, including design and analysis of computer experiments (Santner *et al.*, 2003), simulation modeling (Ankenman *et al.*, 2010), and optimization (Huang *et al.*, 2006). In addition, it is particularly useful in the modeling of spatially

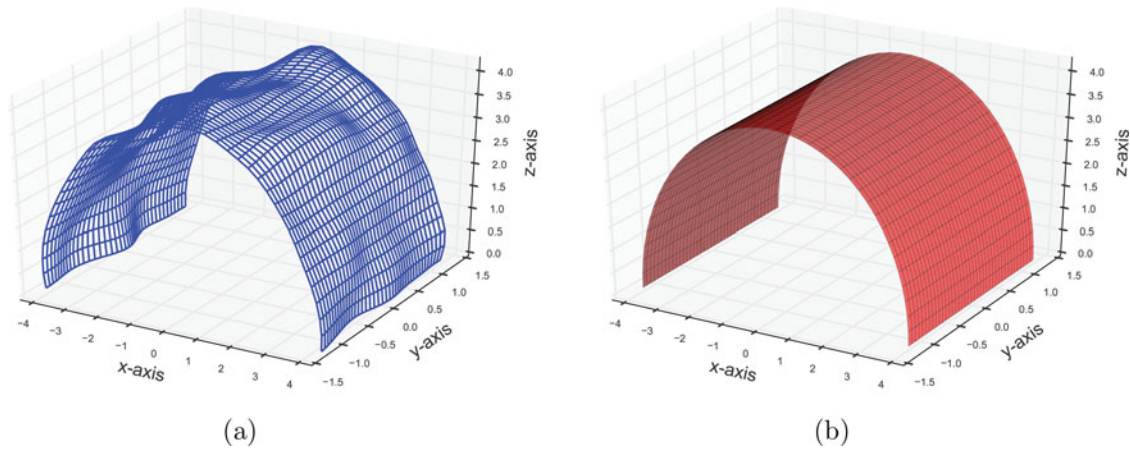


**Figure 1.** Comparison between the original and fitted profiles: (a) the original tunnel and (b) the fitted cylinder model.

correlated data, due to the nature of the GP's working principles. In fact, the GP has been used to model other surface profiles resulting from a material removal process, such as a silicon wafer's surface profile in semiconductor manufacturing (Jin *et al.*, 2012; Plumlee *et al.*, 2013; Zhang *et al.*, 2016). In terms of modeling cylindrical profiles, Colosimo *et al.* (2014) demonstrated an application where the GP was applied to reconstruct a cylindrical surface based on grid sampling measurements. Furthermore, Del Castillo *et al.* (2015) proposed a geodesic GP model to reconstruct free-form surfaces by transforming Cartesian coordinates into machined surface coordinates. These studies demonstrate the key advantage of the GP: it is flexible enough to be able to distinguish the actual feature (or equivalently the local variability) from the designed perfect cylinder. This advantage allows subsequent analyses, such as form error assessment (Xia *et al.*, 2008) and surface monitoring (Colosimo *et al.*, 2014), which are extremely useful in the detection of tunnel deformations.

In practice, however, the applicability of GP modeling is challenging, as the data obtained using the TLS technique are often contaminated with noise or errors, as discussed in Reshetyuk (2006). There are two main sources of errors encountered during TLS sensing: range error and angular error. The range error is also referred to as measurement noise, which can be accounted for by either tuning the instrument's precision level or statistical approaches based on repeated measurements. The angular error, however, has received much less attention. In more

detail, define  $\mathcal{X}^c$  as a point on the tunnel's surface in a Cartesian coordinate system. The TLS measurement system is actually a spherical coordinate system. It includes the distance of  $\mathcal{X}^c$  from the origin (i.e., the position of the scanner),  $\rho$ , and two angles. The first is the azimuthal angle  $\varphi$  in the radial perspective; i.e., the angle between  $\mathcal{X}^c$  and the  $x$ - $y$  plane. The second is the elevation angle  $\theta$  in the axial perspective; i.e., the angle between  $\mathcal{X}^c$  and the  $x$ - $z$  plane, as demonstrated in Figure 2(a). During the TLS survey, the measurements usually cannot be taken exactly at designed coordinates, due to machine and environmental factors, such as tolerances of the rotation joints (Marshall and Stutz, 2011) or tunnel boring machine (TBM) vibration (Reshetyuk, 2006). These angular errors ( $\Delta\varphi$ ,  $\Delta\theta$  in Fig. 2(b) and Fig. 2(c)) are often unobservable, yet have a tremendous impact on the modeling accuracy of a tunnel's profile.

To demonstrate the impact of such angular errors, which we refer to as coordinate errors hereafter, we use a one-dimensional example shown in Figure 3(a) for illustration. We intend to measure the height  $y = f(x)$  marked by the star at the designed location  $x$ . However, the real measurement shifts to  $x + \Delta x$ . As  $\Delta x$  is unobservable, we record the actual measurement  $f(x + \Delta x)$  marked by the circle as if it is still measured at our designed location  $x$ , which results in the recorded value marked by the square. If we use error-contaminated measurements  $(x_i, f(x_i + \Delta x_i))$  to predict the profile, as we can observe in Figure 3(b), there is a significant bias between the predicted profile and the true profile.

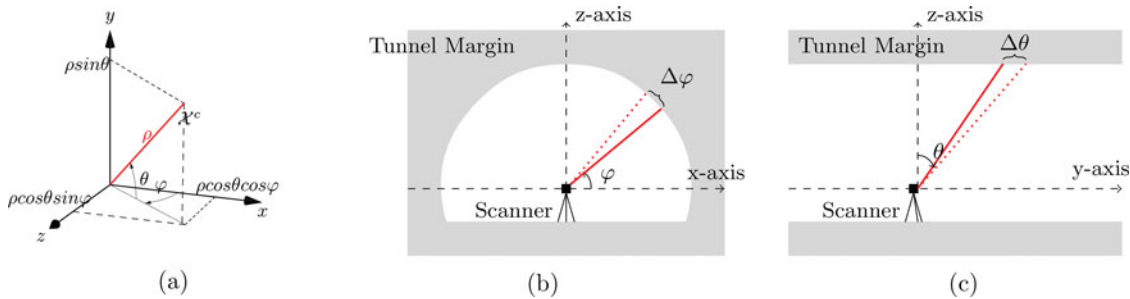


**Figure 2.** Demonstration of the TLS coordinate errors: (a) is the three-dimensional plot where  $\mathcal{X}^c$  is a point on the surface in the Cartesian coordinate system.  $\rho$  is the distance of  $\mathcal{X}^c$  from the original point (i.e., the position of the scanner).  $\varphi$  is the azimuthal angle of  $\mathcal{X}^c$  in the radial perspective; i.e., the angle between  $\mathcal{X}^c$  and the  $x$ - $y$  plane.  $\theta$  is the elevation angle of  $\mathcal{X}^c$  in the axial perspective; i.e., the angle between  $\mathcal{X}^c$  and the  $x$ - $z$  plane. Consequently,  $\mathcal{X}^c = \rho \times [\cos\theta \cos\varphi, \sin\theta, \cos\theta \sin\varphi]^T$ . In (b), the red line is the projection of  $\mathcal{X}^c$  on the  $x$ - $z$  plane, and the angle  $\Delta\varphi$  demonstrates the azimuthal error. In (c), the red line is the projection of  $\mathcal{X}^c$  on the  $y$ - $z$  plane, and the angle  $\Delta\theta$  demonstrates the elevation error.

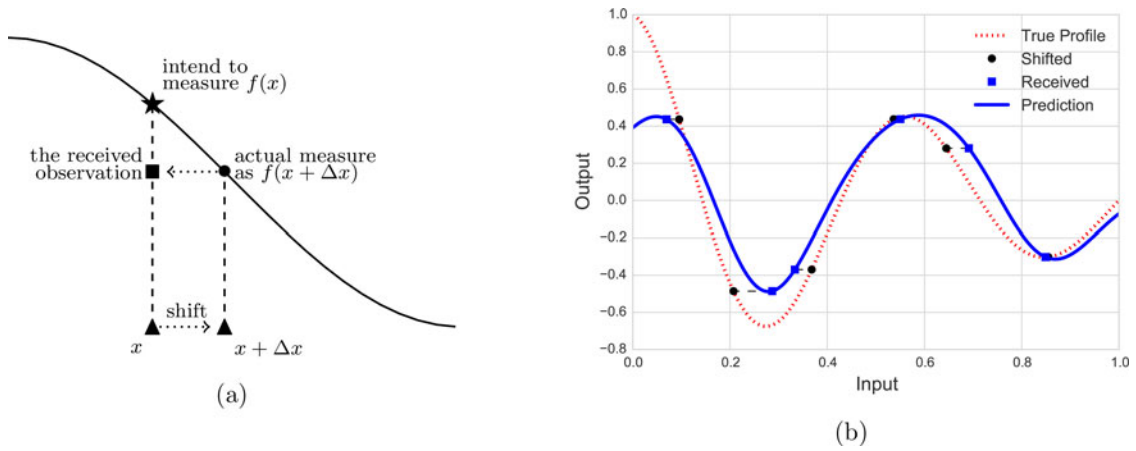


**Figure 3.** Measurement and regression in the presence of coordinate errors: (a) how we observe the measurements and (b) prediction with error-contaminated measurements.

Therefore, it is of great importance to account for the coordinate errors in the GP model to obtain a robust prediction. In the literature on regression, this problem is also acknowledged as Berkson's Error-In-Variable (EIV) problem (Berkson, 1950). Although inferences on Berkson errors in linear models have been thoroughly discussed in the literature (Van Goslign *et al.*, 2006; Fuller, 2009), for nonlinear models, the inferences are few. Most of these inferences use the conditional moments of the responses given the observed predictors to identify the regression coefficients and the input error distribution. Examples include the regression calibration method of Carroll *et al.* (2006) for generalized linear regressions, the iterative re-weighted least squares approach of Huwang and Huang (2000) for polynomial regressions, the quasi-likelihood estimation method of Carroll and Stefanski (1990) for general input errors, and the minimum distance estimator of Wang (2004) for general nonlinear regressions. However, unless the nonlinear regressions have simple forms, in many cases, such as the GP, their conditional moments have no analytical solution. Then the above methods require significant computational effort to calculate either multiple integrals or to estimate moments by simulation. This hinders their efficient applications in the GP, especially for high-dimensional cases with a lot of sampling points. As for EIV models particularly designed for GP regressions, unfortunately so far all of them focus on classic input errors. For example, Goldberg *et al.* (1997), Kersting *et al.* (2007), and Titsias and Lázaro-gredilla (2011) proposed the use of a heteroscedastic GP for approximation. They suggested using a Taylor expansion to approximate the GP around  $\mathbf{x}_i$  and derived a correction for the prediction proportional to the gradient of the GP. However, since the Berkson error is fundamentally different from classic errors and requires completely different procedures in parameter estimation and inference, the above methods cannot be applied to this situation.

To fill in the research gap in modeling tunnel profiles, we propose a GP with error adjustments to model complex tunnel profiles in the presence of coordinate errors. Our contributions are twofold. First, we apply the GP to tunnel profile modeling. The key to its implementation is to obtain an accurate GP model representation. Compared with other existing methods in the literature, the proposed GP has more flexibility to describe local

variability and the spatial correlation structure of the tunnel surface. Consequently, the GP can capture gradual minor deformations more efficiently in their early stages. Furthermore, our method is easy to generalize and implement in other types of engineering surfaces. That is of interest itself. Second, we consider modeling the profile in the presence of coordinate errors. In particular, we propose a new method to deal with error contamination. The key process is to treat coordinate errors as additional information, with the help of which the gradient of the GP can be closely estimated. Then we can incorporate the gradient information into the profile modeling to provide a more accurate approximation. Actually, the GP has the unique advantage including gradients into the estimation, which can be conveniently achieved by the direct gradient-enhanced GP (Chung and Alonso, 2002; Zimmermann, 2013; Ulaganathan *et al.*, 2016). However, the traditional gradient-enhanced GP in the literature supposes that gradient information is known in advance from finite-difference methods or adjoint-based methods (Chung and Alonso, 2002; Dwight and Han, 2009). Unfortunately, in our case, gradient information is unknown and has to be inferred. With this in mind, we propose an iterative algorithm that allows us to simultaneously learn gradient information together with the GP. After convergence of the algorithm, the information on coordinate errors is added to the GP model. Consequently, the information loss caused by the error is mitigated. The numerical results show that the prediction of the proposed GP is robust against coordinate errors and is more accurate than existing approaches. Based on the proposed model, some potential monitoring schemes can be developed in future. Our model hopes to shed light upon this research field.

The remainder of this article is organized as follows. Section 2 introduces the reading-surface, based on which a general framework of modeling a tunnel's profile using the GP is presented. Section 3 discusses a modified GP model for robust prediction with error-adjusted estimation to account for coordinate errors. Section 4 validates our model through simulation studies and applies our method in a real case study to demonstrate the effectiveness and applicability of our method. Finally, Section 5 concludes this study and discusses future research directions.



## 2. GP model for a tunnel's profile

### 2.1. Reading-surface profile

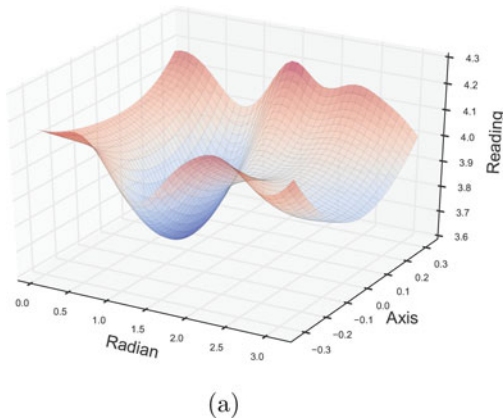
Objects on a tunnel's surface are measured by TLS. The scanner is set up at the central axis of the tunnel via a preliminary registration procedure. The measurements are recorded in a spherical coordinate system. This coordinate system is demonstrated in Figure 2. Specifically, we let  $\mathcal{X} \equiv [\rho, \varphi, \theta]^T$  denote a three-dimensional point on the tunnel's surface in the spherical coordinate system, where  $\rho$  is the reading of the distance measurement from the scanner to the tunnel surface,  $\varphi$  is the azimuthal angle in radial perspective, and  $\theta$  is the elevation angle in the axial perspective.

In TLS scanning,  $\varphi$  and  $\theta$  are controllable variables that are inputted to the scanning system. The scanner then rotates as instructed to position  $[\varphi, \theta]^T$ , takes measurements, and records the distance readings. In this context, we define a function  $\rho = f(\mathbf{x}) : \mathbb{R}^2 \mapsto \mathbb{R}$  that maps the measurement coordinates  $\mathbf{x} \equiv [\varphi, \theta]^T$  to the distance reading  $\rho$ . This function is demonstrated as a surface profile in Figure 4(a). We name such an  $f(\mathbf{x})$  as a reading-surface. Each reading-surface uniquely determines a three-dimensional tunnel profile in the Cartesian coordinate system through simple coordinate transformation. Let  $\mathcal{X}^c = \rho \times [\cos \theta \cos \varphi, \sin \theta, \cos \theta \sin \varphi]^T$  denote a point on the surface in the Cartesian coordinate system. Figure 4(b) shows the transformed three-dimensional tunnel profile. Consequently, modeling the tunnel profile is equivalent to modeling the reading-surface.

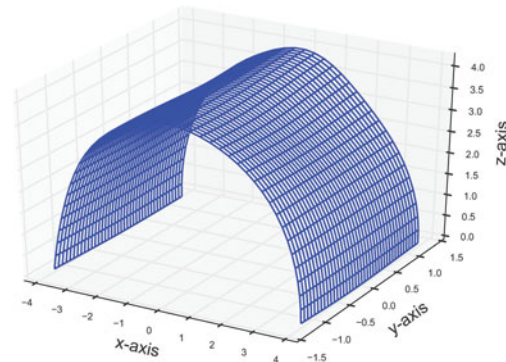
**Remark 1.** The above-described spherical coordinate system is local to the scanner. When multiple scanners are used collaboratively, we could transform the local coordinates to global ones by simply letting  $\mathcal{X}^g = \mathbf{p} + \mathbf{R} \times \mathcal{X}^c$ , where  $\mathcal{X}^g$  is the point on the global surface,  $\mathbf{p}$  is the position of the current scanner, and  $\mathbf{R}$  is a rotation matrix. For demonstration purposes, in this study, we focus on modeling a tunnel segment with a single scanner.

### 2.2. GP model

We propose the following GP model representation to approximate the reading-surface. Similar to the treatment of Xia *et al.* (2008), we decompose the reading-surface into two parts:



(a)



(b)

Figure 4. Example of the reading-surface transformation: (a) a reading-surface profile and (b) the corresponding tunnel profile.

$$f(\mathbf{x}) = r(\mathbf{x}) + z(\mathbf{x}), \quad (1)$$

where  $r(\mathbf{x})$  is the designed profile, and  $z(\mathbf{x})$  denotes the local variability of the tunnel's surface from the standard cylindrical shape due to deformation. Intuitively,  $r(\mathbf{x})$  represents the desired reading-surface in the perfect scenario that the tunnel has an exact cylindrical shape. Therefore, given the designed tunnel radius  $\alpha$ ,  $r(\mathbf{x})$  only depends on  $\theta$  as  $r(\mathbf{x}) = \alpha / \cos(\theta)$ .

On the other hand, the local variability  $z(\mathbf{x})$  is usually unknown and needs to be estimated from the measurements. We assume  $z(\mathbf{x})$  is a realization of a GP with mean function  $\mu$  and covariance function  $k(\cdot, \cdot)$ . In particular, suppose that we have collected  $n$  distance readings  $\boldsymbol{\rho} \equiv [\rho_1, \rho_2, \dots, \rho_n]^T$  at corresponding coordinates  $\mathbf{X} \equiv [\mathbf{x}_1, \mathbf{x}_2, \dots, \mathbf{x}_n]^T$ . Based on Equation (1), we assume  $\boldsymbol{\rho} - r(\mathbf{X})$  follows a multivariate normal distribution with the  $n$ -by-1 mean vector  $\mu \mathbf{1}_n$  and  $n$ -by- $n$  covariance matrix  $\boldsymbol{\Sigma}_0$ , whose  $ij$ th element is defined as  $k(\mathbf{x}_i, \mathbf{x}_j)$ ; that is,

$$\boldsymbol{\rho} - r(\mathbf{X}) | \mathbf{X} \sim \mathcal{N}(\mu \mathbf{1}_n, \boldsymbol{\Sigma}_0). \quad (2)$$

To describe the spatial correlation between points on the tunnel's surface, we assume that the covariance between two arbitrary points  $\mathcal{X}, \mathcal{X}'$  on the tunnel's surface fully depends on the Euclidean distance  $d$  of  $\mathbf{x}$  and  $\mathbf{x}'$ . With this in mind, we further decompose this distance  $d$  into two orthogonal projections as shown in Figure 5.

- In the radial perspective (Fig. 5(a)), the distance projected on the  $x$ -axis can be expressed as  $d_x = |\rho \cos \theta \cos \varphi - \rho' \cos \theta' \cos \varphi'|$ , whereas the one projected on the  $z$ -axis is  $d_z = |\rho \cos \theta \sin \varphi - \rho' \cos \theta' \sin \varphi'|$ . As  $\rho$  and  $\rho'$  are unknown until we take measurements, we could use their designed values  $r(\theta), r(\theta')$  instead. Hence, we obtain:

$$d_x = |\alpha \cos \varphi - \alpha \cos \varphi'|, \quad (3)$$

$$d_z = |\alpha \sin \varphi - \alpha \sin \varphi'|. \quad (4)$$

- In axial perspective (Fig. 5(b)), similarly we could obtain the projected distance:

$$d_y = |\alpha \tan \theta - \alpha \tan \theta'|. \quad (5)$$

Then we can design  $k(\mathbf{x}, \mathbf{x}')$  as a function of  $d_x, d_y$ , and  $d_z$ . Generally for GP modeling,  $k(\mathbf{x}, \mathbf{x}')$  is assumed to have a parametric form, such as the power exponential, the rational

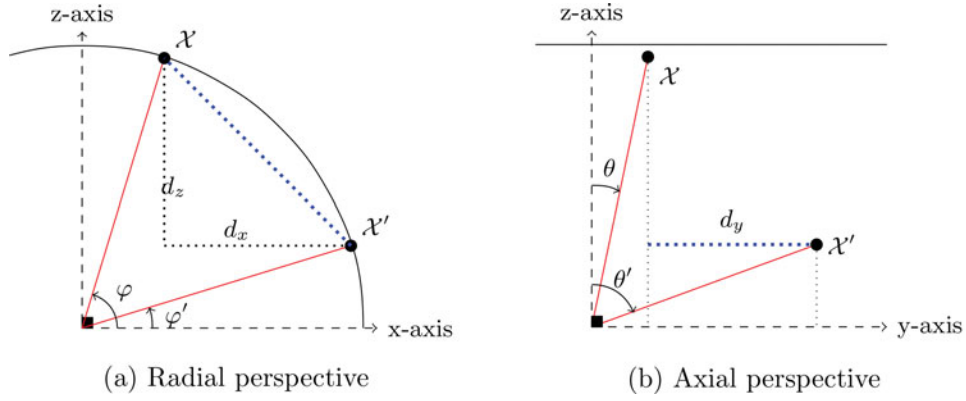


Figure 5. Projected distance between two points on the tunnel surface: (a) from the radial perspective and (b) from the axial perspective.

quadratic, or the Matérn family. Here we assume that the tunnel's profile is smooth and continuous and propose to use the Gaussian correlation function in the analysis. The Gaussian correlation function also has the good property that any arbitrary smooth function can be constructed as a regression model with the Gaussian covariance functions (MacKay, 1998). Of course, when the smoothness assumption is not satisfied, other types of correlation functions with more flexibility can be applied in our model, which is further discussed in Remark 3. To represent anisotropic spatial correlation effects, we assign three length-scale parameters  $l_x$ ,  $l_y$ , and  $l_z$  to the projected distances, respectively. Hence, the covariance between  $\mathcal{X}$  and  $\mathcal{X}'$  becomes

$$k(\mathbf{x}, \mathbf{x}') = \sigma_f^2 \exp \left[ -\left( \frac{d_x}{l_x} \right)^2 - \left( \frac{d_y}{l_y} \right)^2 - \left( \frac{d_z}{l_z} \right)^2 \right], \quad (6)$$

where  $\sigma_f^2$  is the overall surface variance. Other than the Euclidean distance, the geodesic distance suggested by Del Castillo *et al.* (2015) is another alternative to use in the covariance function.

Now the GP model has five parameters. Specifically, we let  $\Theta \equiv [\mu, \sigma_f^2, l_x, l_y, l_z]^T$  denote the entire parameter set. When  $\Theta$  is unknown, it can be estimated from the measurements  $(\rho, \mathbf{X})$  by maximizing the log-likelihood function (up to a constant)

$$\hat{\Theta} = \arg \max_{\Theta} \left( -\frac{1}{2} \log |\Sigma_0| - \frac{1}{2} \mathbf{e}^T \Sigma_0^{-1} \mathbf{e} \right), \quad (7)$$

where  $\mathbf{e} = \rho - \mu \mathbf{1}_n - r(\mathbf{X})$ . The optimization problem in Equation (7) can be solved numerically. Please refer to Appendix A-I for more technical details.

Given  $\Theta$  (or estimated from historical data), and conditional on  $\mathbf{X}$  and  $\rho$ , the reading-surface  $f(\mathbf{x}^*)$  at any unmeasured coordinates  $\mathbf{x}^*$  will still follow a normal distribution and can be predicted as

$$\mathbb{E}[f(\mathbf{x}^*) | \mathbf{X}, \rho] = \mu + r(\mathbf{x}^*) + \Sigma_{*,0} \Sigma_0^{-1} \mathbf{e}, \quad (8)$$

$$\mathbb{V}[f(\mathbf{x}^*) | \mathbf{X}, \rho] = \Sigma_* - \Sigma_{*,0} \Sigma_0^{-1} \Sigma_{*,0}^T, \quad (9)$$

where  $\Sigma_* = k(\mathbf{x}^*, \mathbf{x}^*)$  is the variance at point  $\mathbf{x}^*$ , and  $\Sigma_{*,0}$  is a 1-by- $n$  vector consisting of  $k(\mathbf{x}^*, \mathbf{x}_i)$  for each element  $\mathbf{x}_i$ ,  $i = 1, 2, \dots, n$  in  $\mathbf{X}$ . Equation (8) provides a prediction of the reading-surface at any location, whereas Equation (9) quantifies the prediction uncertainty. Using this prediction, we can obtain the entire reading-surface, which can be transformed to the tunnel profile.

In summary, the GP modeling framework adapts a measure-a-few-and-predict-the-rest work flow. It can efficiently produce a continuous representation of the whole tunnel surface while still being flexible and able to accurately capture the local variability.

**Remark 2.** By using Equation (1), we assume that the scanner's reading is accurate. In practice, however, measurement noise may exist. It has been reported in the literature that measurement noise depends on the incident angle  $\theta$  (Reshetyuk, 2006; Delaloye *et al.*, 2011). When measurement noise is present, we can fit the GP model with noisy observations (Rasmussen and Williams, 2006) by simply substituting  $\Sigma_0$  by  $\Sigma_0 + \Lambda_0$ , where  $\Lambda_0$  is a diagonal matrix containing the noise variance. On the other hand, as the noise depends on incident angle, empirically we could control  $\theta$  to be in the range  $[-0.45, 0.45]$  (in radians). Under this condition the noise becomes negligible compared with other variables.

### 3. Estimation with coordinate errors

In Section 2.1, we introduced the two controlled variables in the TLS technique:  $\varphi$  and  $\theta$ . In practice, measurements are not usually taken at the exact designated locations  $[\varphi, \theta]^T$ . Instead, the measurement position may shift to  $[\varphi + \Delta\varphi, \theta + \Delta\theta]^T$  due to equipment vibration, as demonstrated in Figure 2. Here  $\Delta\varphi$ ,  $\Delta\theta$  are random and unobservable. Without much prior information, we treat them as Gaussian noise; i.e.,  $\Delta\mathbf{x} \equiv [\Delta\varphi, \Delta\theta]^T \sim \mathcal{N}(\mathbf{0}, \Sigma_\Delta)$ . The scale of  $\Sigma_\Delta$  is usually estimated during instrument calibration.

When  $\Delta\mathbf{x}$  is present, the TLS reading will be contaminated, as  $\tilde{\rho} = f(\mathbf{x} + \Delta\mathbf{x})$  instead of  $f(\mathbf{x})$ . Since  $\Delta\mathbf{x}$  is random and unknown, it becomes challenging to estimate  $f(\cdot)$  using contaminated observations  $\langle \mathbf{x}, \tilde{\rho} \rangle$ . Fortunately, due to the fast sensing capability of TLS, we can take multiple measurements at each designed location. These "repeated" measurements provide valuable and more accurate information on the  $f(\cdot)$ . To illustrate, we use a one-dimensional example shown in Figure 6. In Figure 6(a), we take multiple measurements at each designed position  $\mathbf{x}_i$ :

$$\tilde{\rho}_{ij} = f(\mathbf{x}_i + \Delta\mathbf{x}_{ij}), \quad j = 1, 2, \dots, m_i. \quad (10)$$

However, as the  $\Delta\mathbf{x}_{ij}$  are unknown, what we perceive are a sequence of observation pairs  $\langle \mathbf{x}_i, \tilde{\rho}_{ij} \rangle$ ,  $i = 1, \dots, n$ ,

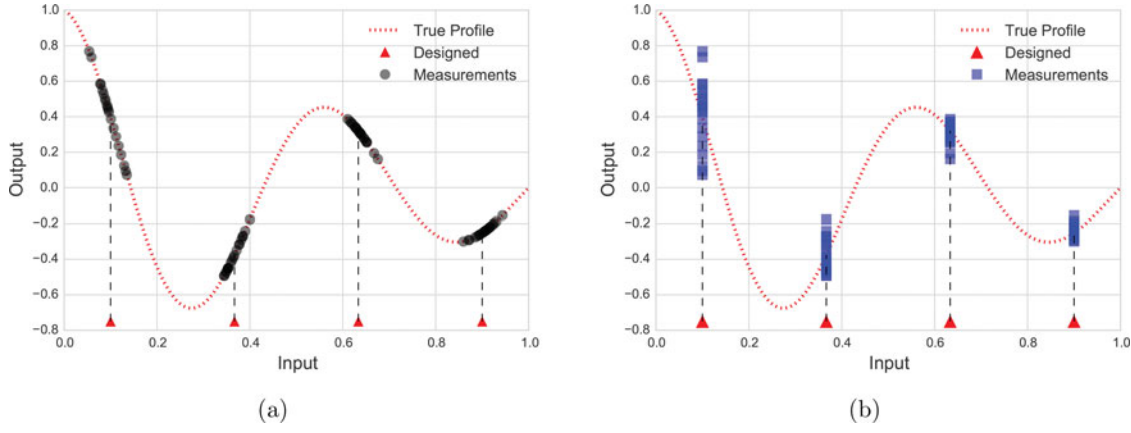


**Figure 6.** Repeated measurements scheme: (a) real measurements around designed coordinates marked by dashed lines and (b) received measurements as replications at designed coordinates.

$j = 1, \dots, m_i$  as demonstrated in Figure 6(b). In other words, the multiple measurements taken at a single designed position are perceived as “repeated” measurements, even if they are actually taken at different positions. Even though we cannot obtain the exact position  $\mathbf{x}_i + \Delta \mathbf{x}_{ij}$ , these “repeated” measurements are still informative. The simplest revision is to take the average of the repeat samples,  $\sum_{j=1}^{m_i} \tilde{\rho}_{ij}/m_i$ , and use it to closely approximate the function value at  $\mathbf{x}_i$ . This method can reduce the estimation standard deviation by a factor of  $\sqrt{n}$  (Ramoni and Anagnostou, 2011). However, a cleverer method is to take the variance of  $\tilde{\rho}_{ij}$  into account as well, since it provides important information on the derivatives of  $f(\cdot)$  at location  $\mathbf{x}_i$ . As clearly demonstrated in Figure 6(b), at the location where the curve has a larger derivative, the variance of  $\tilde{\rho}_{ij}$  is also larger. As a result, we hope to utilize the information on the function value and its gradient from the “repeated” measurements together, in order to obtain a more accurate estimation of the tunnel profile.

Actually, the gradient-enhanced GP has been commonly used to improve the estimation performance of a GP (Chung and Alonso, 2002; Zimmermann, 2013; Ulaganathan *et al.*, 2016). However, the traditional gradient-enhanced GP models in the literature assume that information about the gradient is known primarily from finite-difference methods or adjoint-based methods (Chung and Alonso, 2002; Dwight and Han, 2009), whereas in our case, the gradient information is unknown. Therefore, the key procedure is to estimate the gradient from the repeated measurements, which will be introduced later.

### 3.1. Estimating gradients from repeated measurements

In this part, we provide technical details on how to derive the gradient of  $f(\cdot)$  at location  $\mathbf{x}_i$  based on the repeated measurements.

Given that the tunnel profile  $f(\cdot)$  is twice differentiable (see Remark 3 for further discussion), we can apply a first-order Taylor expansion  $f(\mathbf{x}_i + \Delta \mathbf{x}_i) \approx f(\mathbf{x}_i) + \nabla f(\mathbf{x}_i)^T \Delta \mathbf{x}_i$ , where  $\nabla f(\mathbf{x}_i) = [\partial f(\mathbf{x}_i)/\partial \varphi_i, \partial f(\mathbf{x}_i)/\partial \theta_i]^T$  are the derivatives of  $f(\cdot)$  with respect to  $\varphi$  and  $\theta$ . As we assume  $\Delta \mathbf{x}_i \sim \mathcal{N}(\mathbf{0}, \Sigma_\Delta)$ , taking expectation and variance with respect to  $\Delta \mathbf{x}_i$  on both sides of the Taylor approximation, we can obtain

$$\mathbb{E}[f(\mathbf{x}_i + \Delta \mathbf{x}_i)] \approx \mathbb{E}[f(\mathbf{x}_i) + \nabla f(\mathbf{x}_i)^T \Delta \mathbf{x}_i] = f(\mathbf{x}_i), \quad (11)$$

$$\begin{aligned} \mathbb{V}[f(\mathbf{x}_i + \Delta \mathbf{x}_i)] &\approx \mathbb{V}[f(\mathbf{x}_i) + \nabla f(\mathbf{x}_i)^T \Delta \mathbf{x}_i] \\ &= \nabla f(\mathbf{x}_i)^T \Sigma_\Delta \nabla f(\mathbf{x}_i). \end{aligned} \quad (12)$$

According to Taylor’s theorem, the truncated approximation error is  $\mathbb{E}[\Delta \mathbf{x}_i^T \mathbf{H}(\xi) \Delta \mathbf{x}_i/2]$ , where  $\mathbf{H}(\xi)$  is the Hessian matrix of  $f$  at  $\xi$ , and  $\xi$  is somewhere between  $\mathbf{x}_i$  and the realization  $\mathbf{x}_i + \Delta \mathbf{x}_{ij}$ . In other words, as long as the function  $f(\cdot)$  is not highly nonlinear and the  $\Delta \mathbf{x}_{ij}$  are small, the first-order Taylor approximation can provide satisfactory accuracy.

Therefore, we could use the sample statistics of the “repeated” measurements to estimate  $f(\mathbf{x}_i)$  and  $\nabla f(\mathbf{x}_i)$  based on Equations (11) and (12). In particular, we denote the sample mean  $M_i$  and sample variance  $S_i^2$  from the “repeated” measurements at location  $\mathbf{x}_i$  as

$$M_i = \sum_{j=1}^{m_i} \frac{f(\mathbf{x}_i + \Delta \mathbf{x}_{ij})}{m_i}, \quad (13)$$

$$S_i^2 = \sum_{j=1}^{m_i} \frac{[f(\mathbf{x}_i + \Delta \mathbf{x}_{ij}) - M_i]^2}{m_i - 1}. \quad (14)$$

As a result, a simple estimate of  $\hat{\rho}_i$  is  $M_i$ , with the estimation variance  $\sigma_{\hat{\rho}_i}^2 = S_i^2/m_i$ .

The estimate of  $\nabla f(\mathbf{x}_i)$  is more difficult to obtain from Equation (12). Without loss of generality, we assume  $\Delta \varphi_i$  and  $\Delta \theta_i$  are independent, and  $\sigma_\varphi^2, \sigma_\theta^2$  are the diagonal elements of  $\Sigma_\Delta$ . As a result, Equation (12) can be expressed as

$$\mathbb{V}[f(\mathbf{x}_i + \Delta \mathbf{x}_i)] = \left[ \frac{\partial f(\mathbf{x}_i)}{\partial \varphi_i} \right]^2 \sigma_\varphi^2 + \left[ \frac{\partial f(\mathbf{x}_i)}{\partial \theta_i} \right]^2 \sigma_\theta^2. \quad (15)$$

Define the ratio

$$\tau_i = \frac{\partial f(\mathbf{x}_i)}{\partial \theta_i} \bigg/ \frac{\partial f(\mathbf{x}_i)}{\partial \varphi_i}$$

and we can obtain the gradient estimates

$$\left| \frac{\partial \hat{f}(\mathbf{x}_i)}{\partial \varphi_i} \right| = \frac{S_i}{\sqrt{\sigma_\varphi^2 + \tau_i^2 \sigma_\theta^2}}, \quad \left| \frac{\partial \hat{f}(\mathbf{x}_i)}{\partial \theta_i} \right| = \tau_i \left| \frac{\partial \hat{f}(\mathbf{x}_i)}{\partial \varphi_i} \right|. \quad (16)$$

In practice,  $\tau_i$  and the signs of the partial derivatives are unknown. To obtain a robust and accurate estimate, we adopt an iterative approach, which will be described in detail at the end of this section. The estimation variance based on

Equation (16) can also be obtained as

$$\begin{aligned} \mathbb{V}\left[\frac{\partial \hat{f}(\mathbf{x}_i)}{\partial \varphi_i}\right] &= \frac{\mathbb{V}[S_i]}{\sigma_\varphi^2 + \tau_i^2 \sigma_\theta^2} = \frac{S_i^2(1 - c_4^2)}{\sigma_\varphi^2 + \tau_i^2 \sigma_\theta^2}, \\ \mathbb{V}\left[\frac{\partial \hat{f}(\mathbf{x}_i)}{\partial \theta_i}\right] &= \tau_i^2 \mathbb{V}\left[\frac{\partial \hat{f}(\mathbf{x}_i)}{\partial \varphi_i}\right], \end{aligned} \quad (17)$$

where  $c_4$  is the unbiased correction constant for sample standard deviation. The expressions of  $c_4$  and  $\mathbb{V}[S]$  are provided in Appendix A-III.

### 3.2. GP prediction with gradient information

Taking the information on both  $\hat{f}(\mathbf{x}_i)$  and  $\nabla \hat{f}(\mathbf{x}_i)$  into account, we can have a better estimation of the tunnel profile compared with the GP of Equation (7), where only function values are considered. We introduce the gradient-enhanced GP in detail as below.

Specifically, let  $\mathbf{D}_\varphi \equiv [\partial f(\mathbf{x}_1)/\partial \varphi_1, \partial f(\mathbf{x}_2)/\partial \varphi_2, \dots, \partial f(\mathbf{x}_n)/\partial \varphi_n]^T$  and  $\mathbf{D}_\theta \equiv [\partial f(\mathbf{x}_1)/\partial \theta_1, \partial f(\mathbf{x}_2)/\partial \theta_2, \dots, \partial f(\mathbf{x}_n)/\partial \theta_n]^T$ . Subsequently, we denote  $\boldsymbol{\rho}_A \equiv [\boldsymbol{\rho}, \mathbf{D}_\varphi, \mathbf{D}_\theta]^T$  as the augmented data that include both the function values and gradients at all designed locations  $\mathbf{x}_i, i = 1, \dots, n$ . If  $f(\mathbf{x})$  follows a GP, then the augmented data  $\boldsymbol{\rho}_A$  also follow a multivariate normal distribution (Santner *et al.*, 2003; Chen *et al.*, 2013), with a  $3n$ -by- $3n$  covariance matrix  $\boldsymbol{\Sigma}_A$  as demonstrated in Figure 7.  $\boldsymbol{\Sigma}_A$  represents the covariance within augmented data  $\boldsymbol{\rho}_A$  based on the GP structure. When  $\boldsymbol{\rho}_A$  are not directly observable but estimated from data as  $\hat{\boldsymbol{\rho}}_A$ , the estimation variance can also be considered, denoted by  $\boldsymbol{\Lambda}_A$  in Figure 7.  $\boldsymbol{\Lambda}_A$  essentially accounts for the estimation error of  $\hat{\boldsymbol{\rho}}_A$  based on Equations (13) and (16). The augmented GP can be estimated by maximizing the log-likelihood function, following the same method as the GP in Section 2.2. Please refer to Appendix A-II for more technical details.

With the estimated GP, by plugging  $\hat{\boldsymbol{\rho}}_A$ ,  $\boldsymbol{\Sigma}_A$ ,  $\boldsymbol{\Lambda}_A$  into Equations (8) and (9), we can obtain the prediction for the entire tunnel profile at any given location  $\mathbf{x}^*$  as

$$\begin{aligned} \mathbb{E}[f(\mathbf{x}^*)|\mathbf{X}, \hat{\boldsymbol{\rho}}_A] &= \mu + r(\mathbf{x}^*) + \boldsymbol{\Sigma}_{*,A}(\boldsymbol{\Sigma}_A + \boldsymbol{\Lambda}_A)^{-1} \mathbf{e}_A, \\ \mathbb{V}[f(\mathbf{x}^*)|\mathbf{X}, \hat{\boldsymbol{\rho}}_A] &= \boldsymbol{\Sigma}_* - \boldsymbol{\Sigma}_{*,A}(\boldsymbol{\Sigma}_A + \boldsymbol{\Lambda}_A)^{-1} \boldsymbol{\Sigma}_{*,A}^T, \end{aligned} \quad (18)$$

where  $\mathbf{e}_A = \hat{\boldsymbol{\rho}}_A - \mu \mathbf{1}_n^A - r_A(\mathbf{X})$  and where  $\mu \mathbf{1}_n^A \equiv [\mu \mathbf{1}_n, \mathbf{0}_{2n}]^T$ ,  $r_A(\mathbf{X}) \equiv [r(\mathbf{X}), \mathbf{0}_{2n}]^T$ , and  $\boldsymbol{\Sigma}_{*,A}$  is the augmented covariance between  $f(\mathbf{x}^*)$  and  $\boldsymbol{\rho}_A$ . Equation (18) hence provides a continuous prediction to  $f(\cdot)$  with quantified prediction uncertainty.

It should be noted that sometimes the measurement system may suffer from output noise. In these cases, many gradient estimation methods will be dramatically infected by the output

noise, such as the finite-difference estimation. Fortunately, our method is still effective in these cases. This is due to our gradient estimation being based on the Taylor expansion of the GP. Our estimation only uses the moment information of coordinate errors but does not use the repeat samples to directly calculate gradients. Therefore, our method does not have this problem.

### 3.3. Implementation procedure

In short, the complete procedure of estimating a two-dimensional tunnel surface profile based on data with coordinate error is now summarized.

We first fit an initial GP model solely using data  $\langle \mathbf{x}_i, M_i \rangle, i = 1, \dots, n$ . Such an initial GP model is also referred to as GP with noisy observations in the literature (Rasmussen and Williams, 2006). Based on the initial GP model, we obtain estimates of all  $\tau_i$ , as well as the directions of the partial derivatives. Then we update the gradient estimates based on Equation (16) and update the GP model with better accuracy. We repeat the above procedures to iteratively refine the estimates of  $\tau_i$  and  $\nabla f(\mathbf{x}_i)$  for further improvement. An algorithmic sketch of the procedure is shown in Algorithm 1.

**Remark 3.** It should be noted that when the profile to be modeled is not sufficiently smooth or continuous to allow the Gaussian correlation function assumption to be satisfied, we may use other types of correlation functions. However, the correlation function must be at least twice differentiable to calculate the correlations between the gradient observations. Due to this restriction, we limit our scope to stationary correlation functions, such as the Matérn family functions. To make the GP path twice differentiable, the degree parameter  $\nu$  of the Matérn correlation functions should be bigger than two (recently Lockwood and Anitescu (2012) showed that  $\nu = 1.5$  is also applicable in the gradient-enhanced GP). A detailed discussion on various differentiable correlation functions is given by N  ther and Šim  k (2003) and Stein (2012). It should be noted that no matter what available correlation function is used in our model, the modeling framework and estimation procedure of Algorithm 1 can be applied with trivial modifications. In particular, we only need to change the first-order and second-order derivatives of  $k(\mathbf{x}, \mathbf{x}')$  based on the chosen correlation function. For the Mat  rn correlation functions, these are discussed in detail in Ulaganathan *et al.* (2016).

## 4. Numerical study

In this section, we first use a one-dimensional numerical example to demonstrate the proposed model. We then present a case

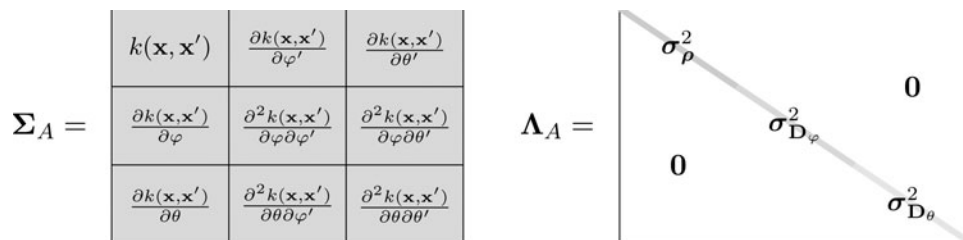


Figure 7. Covariance structure of the GP with estimated function and gradient values.



**Algorithm 1** Fit GP with error-adjusted estimation.Data: Observations  $\mathbf{x}_i$ ,  $f(\mathbf{x}_i + \Delta \mathbf{x}_{ij})$ ,  $i = 1, \dots, n$ ;  $j = 1, \dots, m_i$ Result: GP model with estimated parameters  $\Theta = \{\mu, \sigma_f^2, l_x, l_y, l_z\}$  for the tunnel profile

- 1: Initialize: Set  $k = 0$ ; Estimate the mean  $\hat{\rho} = [M_1, \dots, M_n]$  and fit the initial GP  $f^{(k)}(\cdot; \Theta^{(k)})$  based on data  $\langle \mathbf{x}_i, \hat{\rho}_i \rangle$  using the maximum likelihood method of (A.2) and (A.3).
- 2: Set  $k = k + 1$ , and calculate  $\tau_i^{(k)} = \frac{\partial f^{(k-1)}(\mathbf{x}_i)}{\partial \theta_i} / \frac{\partial f^{(k-1)}(\mathbf{x}_i)}{\partial \varphi_i}$ . Then we get

$$\frac{\partial \hat{f}(\mathbf{x}_i)}{\partial \theta_i} = \text{sgn} \left( \frac{\partial f^{(k-1)}(\mathbf{x}_i)}{\partial \theta_i} \right) \frac{S_i}{\sqrt{\sigma_\varphi^2 + \tau_i^{(k)2} \sigma_\theta^2}}, \quad \frac{\partial \hat{f}(\mathbf{x}_i)}{\partial \varphi_i} = \tau_i^{(k)} \left| \frac{\partial \hat{f}(\mathbf{x}_i)}{\partial \theta_i} \right|.$$

Then we have  $\mathbf{D}_\varphi^{(k)} \equiv [\partial \hat{f}(\mathbf{x}_1)/\partial \varphi_1, \partial \hat{f}(\mathbf{x}_2)/\partial \varphi_2, \dots, \partial \hat{f}(\mathbf{x}_n)/\partial \varphi_n]$ ,  $\mathbf{D}_\theta^{(k)} \equiv [\partial \hat{f}(\mathbf{x}_1)/\partial \theta_1, \partial \hat{f}(\mathbf{x}_2)/\partial \theta_2, \dots, \partial \hat{f}(\mathbf{x}_n)/\partial \theta_n]$ , and the corresponding  $\hat{\rho}_A^{(k)} \equiv [\hat{\rho}, \mathbf{D}_\varphi^{(k)}, \mathbf{D}_\theta^{(k)}]$ .

- 3: Update the GP  $f^{(k)}(\cdot; \Theta^{(k)})$  based on  $\langle \mathbf{x}_i, \hat{\rho}_A^{(k)} \rangle$  using (A.5) and (A.6). where  $\hat{\mathbf{e}} = \hat{\rho} - \hat{\mu}^{(k)} \mathbf{1}_n - r(\mathbf{X})$ .
- 4: if  $\tau_i^{(k)}$  does not converge, go back to Step 2; otherwise, return  $f^{(k)}(\cdot; \Theta^{(k)})$ .

study in which we apply our method to model a tunnel segment in the presence of coordinate errors.

#### 4.1. Predicting the curve profile in the presence of coordinate errors

We use the damped cosine function (Santner *et al.*, 2003):

$$f(x) = \exp(-1.4x) \cos(3.5\pi x), \quad x \in [0, 1] \quad (19)$$

as the testing curve to represent the underlying profile to be predicted. To predict this profile, we followed the procedure described in Section 3.3. First, we generated  $n = 6$  points,  $x_i (i = 1, \dots, 6)$  through Latin-hypercube design—i.e.,  $\mathbf{x} = [0.037, 0.312, 0.368, 0.653, 0.748, 0.935]^T$ —as the designed measurement coordinates. To simulate the coordinate error, we let  $\Delta x \sim \mathcal{N}(0, 0.02)$  and generated  $m = 20$  samples for each site  $x_i$ ,  $i = 1, \dots, 6$ . The measurements were then taken at each  $x_i + \Delta x_i$  but recorded as replications at each  $x_i$ . Using these measurements, we approximated  $f(x_i)$  and the approximation errors  $\sigma_{f_i}^2$  using Equations (13) and (14). Based on these approximations, we fitted the GP model with noisy observations, and the initial prediction is shown in Figure 8(a). As the testing function is one-dimensional, Equation (16) can be simplified to  $|f'(x_i)| = S_i/\sigma_x$  with  $\sigma_x = 0.02$  in this case. Similarly, Equation (17) becomes  $\mathbb{V}[f'(x_i)] = S_i^2(1 - c_4^2)/\sigma_x^2$ . Applying the directions (positive or negative) extracted from Figure 8(a), we obtained the estimations of derivative at each  $x_i$ . These estimations are illustrated in Figure 8(b). We then fitted the GP model with the derivative estimations added. The adjusted prediction is shown in Figure 8(c).

One may notice that by only using noisy observations, the GP model is able to provide a moderate prediction as shown in Figure 8(a). The difference in the models that affects the prediction performance between Figure 8(a) and Figure 8(c) is whether or not we incorporate derivative estimations. As we can observe in Figure 8(c), the prediction approaches the true profile more closely than its rival in Figure 8(a). More quantitatively, we can compare their prediction performances in terms of Mean-Squared Prediction Error (MSPE) evaluated at 1000

equally spaced locations. The MSPE in Figure 8(a) is  $17.52 \times 10^{-3}$ , whereas in Figure 8(c) the MSPE decreases to  $1.25 \times 10^{-3}$ , which indicates a more accurate prediction. Moreover, if we compare the prediction uncertainty represented by the 95% confidence interval band, the prediction in Figure 8(c) is obviously preferable, as the interval band is much narrower. This comparison justifies the necessity of incorporating derivative estimations in the GP model.

The above numerical result was obtained based on six measurement sites and 20 replication at each. We further studied how different sizes for the measurement sites affect the prediction performance in terms of MSPE. We first fixed the replication size  $m = 20$  for every site and varied the size of the measurement sites  $n$  from four to ten. We compared the MSPEs of the GPs with (error adjustment) or without (noisy observations only) derivative estimation. The results are shown in Figure 9(a). We can clearly observe that both MSPEs reduce as the size of the measurement sites increases. This is intuitive, because we obtain more information on the profile when measuring at more sites and thus the prediction tends to be more accurate. In addition, we find that the prediction with the derivative always has a smaller MSPE. This again proves the significance of incorporating derivative estimations.

Second, we fixed the size of the measurement sites  $n = 8$  and varied the replication size  $m$  from 5 to 30 for all sites. The comparison of the MSPE values is shown in Figure 9(b). We can observe that the MSPE of the GP with the derivative slightly decreases as the replication size increases. This is because more replications can give a more accurate estimation on the derivatives. However, we notice that both MSPEs are not so sensitive to the change of  $m$  compared with the first case where we vary  $n$ . This can be explained by the fact that the estimation error has been accounted for in the covariance matrix described in Figure 7. In other words, a moderate number of replications will be sufficient to provide an accurate prediction. When the measurement capability (e.g., total size  $m \times n$ ) is capped, we suggest to allocate more budget on the size of measurement sites for a better prediction performance. Furthermore, it should be noted that although here we only consider coordinate errors, when small output noise exists, our model can still perform very well.

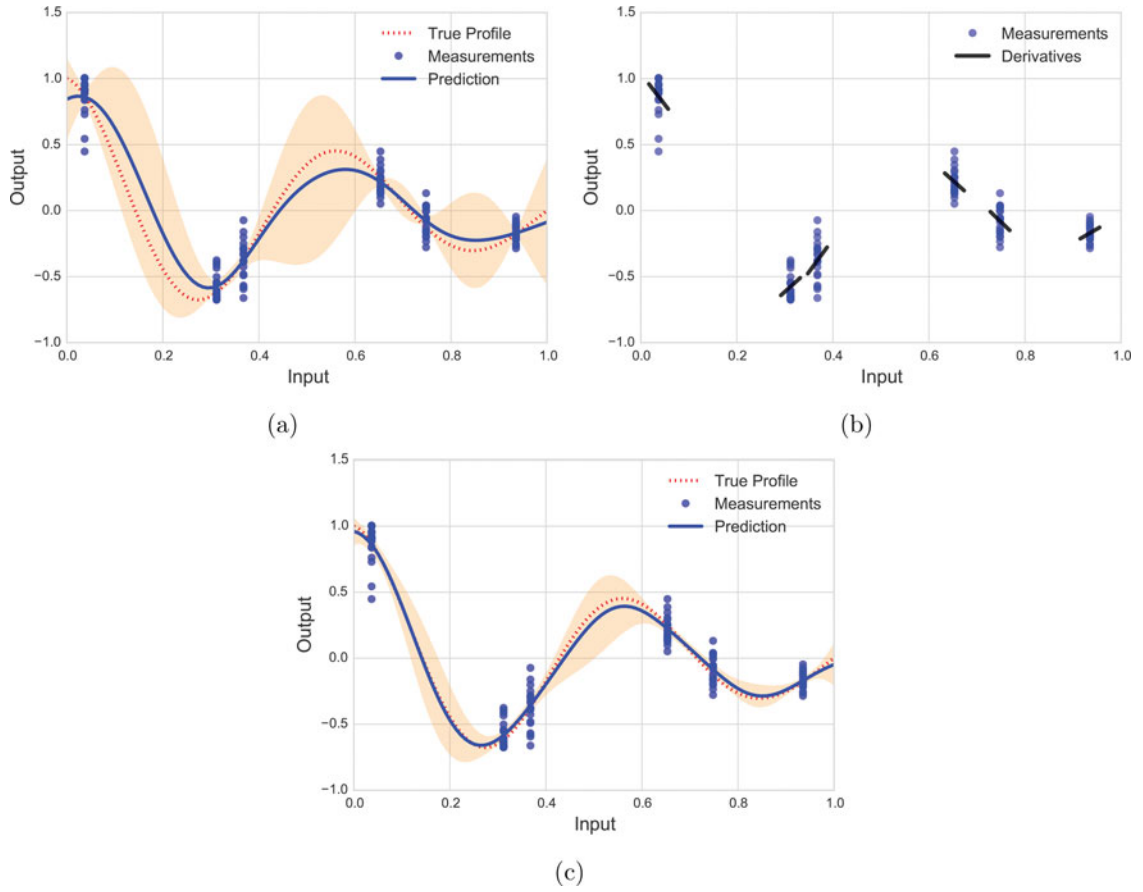


**Figure 8.** Prediction of a curve profile: (a) prediction with noisy observations only; (b) derivative estimations from the repeated measurements; and (c) prediction with derivative estimation. The shaded area denotes the 95% confidence interval band.

#### 4.2. Case study

We applied our proposed method to model a tunnel segment. The designed radius was 5 m along this segment. During its construction, a preliminary scan showed that deformation had occurred, making the real tunnel profile deviate from the designed profile. Therefore, we would like to model the current tunnel profile to monitor the extent of the deformation. This experiment utilized a single TLS, which was set up at the central axis of the segment through the registration procedure. The TLS measured at the surface of the tunnel and recorded the point cloud data to describe the tunnel's profile. Due to

commercial confidentiality issues, we did not directly use the TLS measurements. Instead, based on the TLS results, we used finite element analysis software to reproduce the tunnel's surface. The reproduced data are very close to the original data. Moreover, these data provide a continuous representation of the tunnel's surface and thus can better demonstrate the objective tunnel and help validate our method in this case study. The designed and deformed tunnel surfaces are presented in Figure 10(a), and Figure 10(b) shows the corresponding reading-surface. Our objective is to predict this reading-surface based on sample measurements.

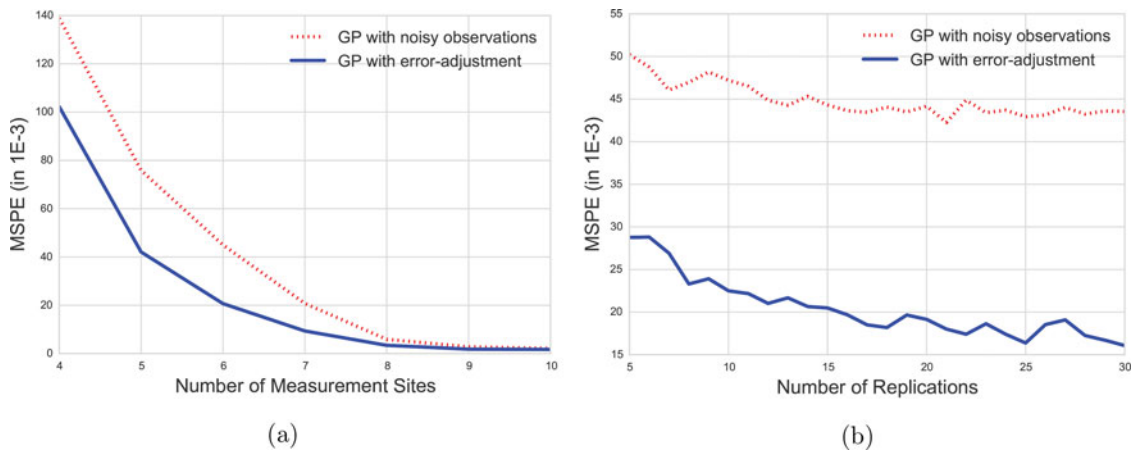


**Figure 9.** MSPE comparison when (a) site size  $n$  varies and (b) replication size  $m$  varies.

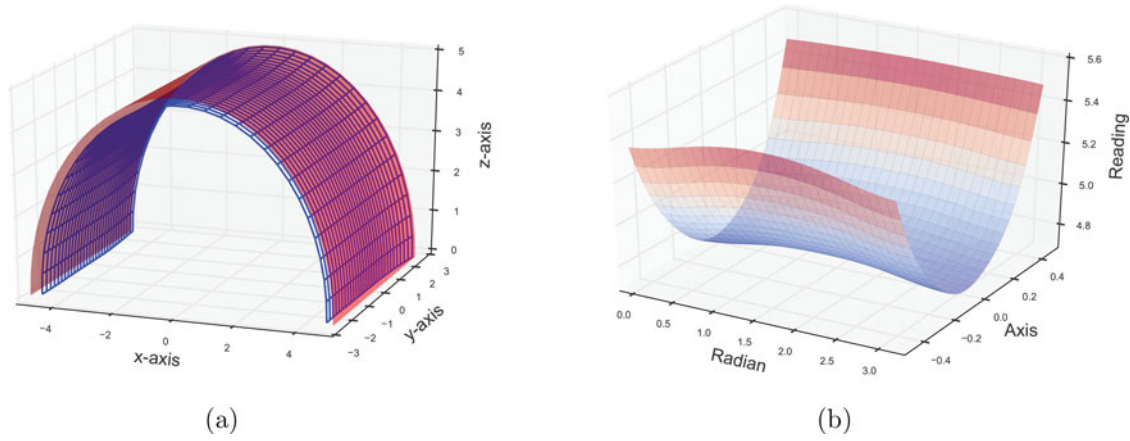


**Figure 10.** The tunnel segment to be modeled: (a) the designed tunnel shown in red surface and the deformed one shown in blue wire frame and (b) the corresponding reading-surface profile.

First, we considered a simple case where the TLS measurements were free from coordinate errors. This simplified case was designed to demonstrate the effectiveness of the GP applied on tunnel profile modeling. To reconstruct the reading-surface, we generated a 20-point equal-distance grid as the designed measurement coordinates. The measurements were sampled from these coordinates and used to fit the GP model using Equation (7). The predicted reading-surface, together with the samples, is presented in Figure 11(b). As a comparison, we applied the existing cylinder-fitting approach (Van Gosliga *et al.*, 2006) to these measurements. The concept that underpins the cylinder-fitting is to find the cylinder's radius such that the sum-squared error from the cylinder to these measurements is minimized. The transformed reading-surface from the fitted cylinder is shown in Figure 11(a). Obviously, the GP-predicted reading-surface is closer to the true one shown in Figure 10(b). Similar to Section 4.1, we quantitatively compare the prediction accuracy through MSPE. The MSPE for the cylinder-fitting prediction is  $5.93 \times 10^{-3}$ . We use it as the benchmark and report the relative MSPE—i.e., the ratio of the model MSPE to this benchmark—to present the fitting improvements. First, we see that the relative MSPE for GP prediction reduces to  $1.58 \times 10^{-2}$ . This significant improvement illustrates that the GP model is a more flexible and accurate process to predict the tunnel's surface.

Second, we considered the case where coordinate error was present and contaminated the TLS measurements. Recall that in Equation (1) we decomposed the reading-surface profile into the designed profile and local variability. This decomposition is demonstrated in Figure 12. Specifically, in this case, the local variability is caused by deformation. Therefore, we refer to the surface in Figure 12(b) as the deformation profile. As the designed profile is constant, modeling the reading-surface is equivalent to modeling the deformation profile. If we ignore the coordinate errors and simply use single-run error-contaminated measurements to fit the GP model, the predicted deformation surface is presented in Figure 13(a). The relative MSPE of this prediction is  $3.88 \times 10^{-2}$ , which is more than twice that of the error-free case. This change clearly shows that the coordinate errors negatively affect the prediction accuracy. To account for this coordinate error, we took repeated measurements at designed locations as proposed in Section 3. Similar to Section 4.1, we compare two GP models. The first GP was fitted using only noisy observations, whereas the latter is our proposed model that combines derivative estimations. Figure 13(b) and Figure 13(c) show the predictions from these two models. The GP with noisy observations gives a relative MSPE of  $2.18 \times 10^{-2}$ , which implies a better accuracy than using single-run measurements. Moreover, the relative MSPE of our proposed method further decreases to  $1.36 \times 10^{-2}$ . The relative

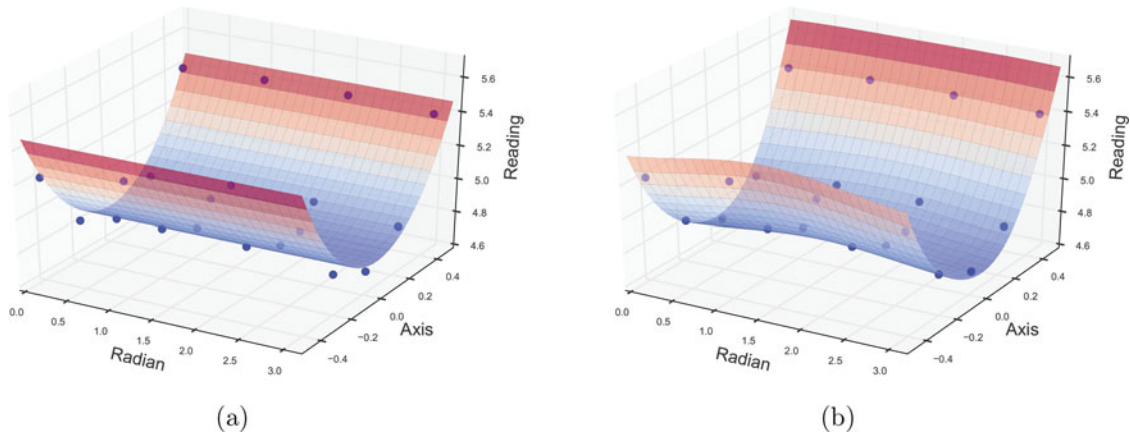


**Figure 11.** Comparison between cylinder-fitting and GP model: (a) cylinder-fitting prediction and (b) GP prediction.

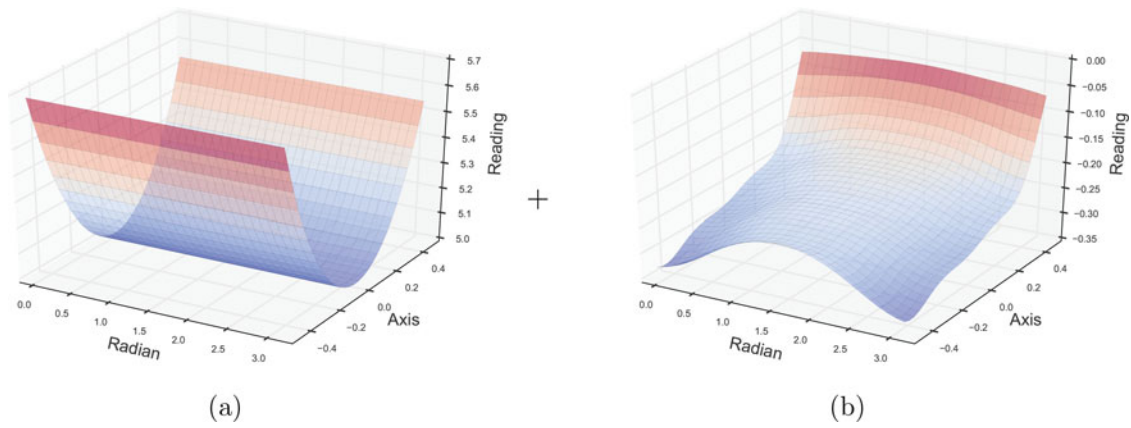


**Figure 12.** Decomposition of the reading-surface profile in Fig. 10(b): (a) the designed profile and (b) the deformation profile.

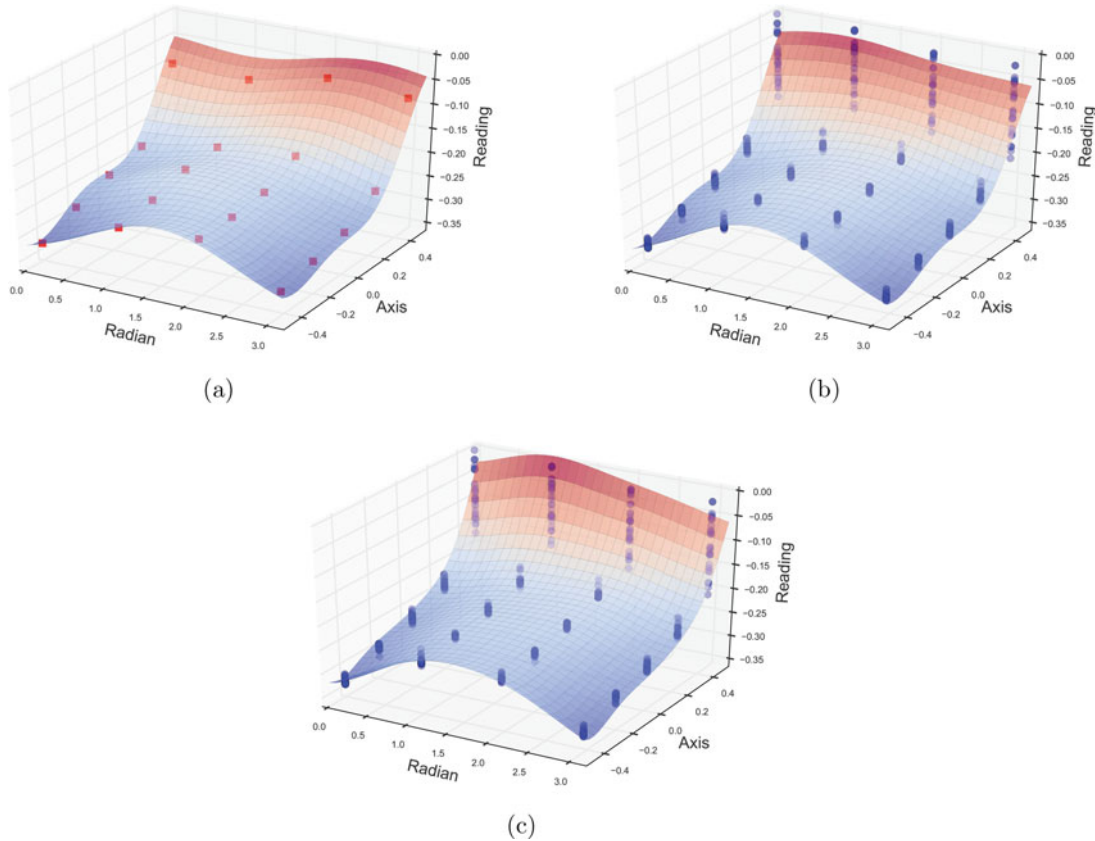


**Figure 13.** Different GP predictions when coordinate errors are present: (a) using single-run measurements; (b) using noisy observations; and (c) combining derivative estimations.

MSPE values for all comparisons in this case study are summarized in Table 1. It is interesting to note that the proposed method has an even lower MSPE in the presence of error than the error-free scenario. This is because with the repeated measurements, the extracted derivative information brings in additional information on the surface and thus contributes to the prediction accuracy. This advantage justifies the effectiveness of using the proposed method.

**Table 1.** The relative MSPE comparison.

Without error		Cylinder-fitting 1	GP model $1.58 \times 10^{-2}$
With error	Single-run $3.88 \times 10^{-2}$	Noisy observations $2.18 \times 10^{-2}$	With derivatives $1.36 \times 10^{-2}$

## 5. Conclusion

This article presents a GP-based approach to reconstruct a tunnel's surface from TLS measurements. We introduce a reading-surface profile that is uniquely transformed from a tunnel profile in the Cartesian coordinate system. Then we apply the GP to model the reading-surface profile. To account for coordinate errors, we take repeated measurements at designed coordinates, from which we can extract mean and gradient information of the reading-surface. The GP model is fitted using both pieces of information, and provides a continuous prediction of the reading-surface that can be finally transformed into the tunnel profile. The numerical results demonstrate that our proposed method is effective and applicable in practice. Therefore, our method has great potential for detecting small deformations in a tunnel's surface.



This work can be extended in several directions. Considering that the GP model is able to quantify the variance of the predicted surface, we could further incorporate statistical tests to develop a more systematic deformation monitoring scheme. For example, we may monitor the GP parameters or the GP fitting residuals. Some existing monitoring schemes for profile data in the GP framework are discussed in Wang *et al.* (2014) and Zhang *et al.* (2016). In addition, our method is currently developed based on static measurements at a certain epoch. If the TLS measurements can be recorded as a time-series, we could further consider a spatiotemporal model to capture the dynamics of the deformation process.

## Acknowledgements

The authors are grateful to the numerous valuable comments provided by the editors and referees.

## Funding

Nan Chen was partially supported by Singapore AcRF Funding R-266-000-085-112 and National Research Foundation Singapore under its Campus for Research Excellence and Technological Enterprise (CREATE). Yong Lei was partially supported by the China 973 Program under Grant 2013CB035405 and the National Natural Science Foundation of China (NSFC) under Grant 51475422.

## Notes on contributors

**Chen Zhang** is a Ph.D. candidate in the Department of Industrial Systems Engineering and Management at National University of Singapore. She received her B.Eng. degree in Electronic Science and Technology (Optics) from Tianjin University. Her research interests include developing new approaches for modeling and monitoring of engineering systems with complex data. She is a member of IISE and INFORMS.

**Yong Lei** is an Associate Professor in the State Key Lab of Fluid Power & Mechatronic Systems, School of Mechanical Engineering at Zhejiang University, China. He obtained his B.S. degree in Automation from Huazhong University of Science and Technology, M.S. degree in Manufacturing Automation from Tsinghua University, and Ph.D. degree in Mechanical Engineering from University of Michigan–Ann Arbor. His research interests include fault diagnosis and condition monitoring of networked industrial automation systems and design, modeling, and control of surgical robotics. He is a member of IEEE and ASME.

**Linmiao Zhang** is a principal data scientist at Micron Technology in Singapore. He received his B.Eng. degree in Industrial Engineering from Nanjing University and his Ph.D. degree in Industrial Systems Engineering and Management from the National University of Singapore. His research topic is statistical modeling of complex engineering data.

**Nan Chen** is an Associate Professor in the Department of Industrial Systems Engineering and Management at the National University of Singapore. He obtained his B.S. degree in Automation from Tsinghua University and M.S. degree in Computer Science, M.S. degree in Statistics, and Ph.D. degree in Industrial Engineering from the University of Wisconsin–Madison. His research interests include statistical modeling and surveillance of service systems, simulation modeling design, condition monitoring, and degradation modeling. He is a member of INFORMS, IISE, and IEEE.

## ORCID

Linmiao Zhang  <http://orcid.org/0000-0002-5884-1377>

## References

Ankenman, B., Nelson, B.L. and Staum, J. (2010) Stochastic kriging for simulation metamodeling. *Operations Research*, **58**, 371–382.

- Berkson, J. (1950) Are there two regressions? *Journal of the American Statistical Association*, **45**, 164–180.
- Carroll, R.J., Ruppert, D., Stefanski, L.A. and Crainiceanu, C.M. (2006) *Measurement Error in Nonlinear Models: A Modern Perspective*, CRC Press, Boca Raton, FL.
- Carroll, R.J. and Stefanski, L.A. (1990) Approximate quasi-likelihood estimation in models with surrogate predictors. *Journal of the American Statistical Association*, **85**, 652–663.
- Chen, X., Ankenman, B.E. and Nelson, B.L. (2013) Enhancing stochastic kriging metamodels with gradient estimators. *Operations Research*, **61**, 512–528.
- Chung, H.-S. and Alonso, J.J. (2002) Using gradients to construct cokriging approximation models for high-dimensional design optimization problems. *40th AIAA Aerospace Sciences Meeting and Exhibit*, 2002-0317, 1–16. AIAA, Reno, NV.
- Colosimo, B.M., Cicorella, P., Pacella, M. and Blaco, M. (2014) From profile to surface monitoring: SPC for cylindrical surfaces via Gaussian processes. *Journal of Quality Technology*, **46**, 95–113.
- Del Castillo, E., Colosimo, B.M. and Tajbakhsh, S.D. (2015) Geodesic Gaussian processes for the parametric reconstruction of a free-form surface. *Technometrics*, **57**, 87–99.
- Delaloye, D., Diederichs, M.S., Walton, G. and Hutchinson, J. (2015) Sensitivity testing of the newly developed elliptical fitting method for the measurement of convergence in tunnels and shafts. *Rock Mechanics and Rock Engineering*, **48**, 651–667.
- Delaloye, D., Hutchinson, J. and Diederichs, M. (2011) Accuracy issues associated with Lidar scanning for tunnel deformation monitoring. in *Proceedings of the 2011 Pan-AM CGS Geotechnical Conference*, Canadian Geotechnical Society, Toronto, Ontario, Canada, pp. 1–6.
- Dwight, R.P. and Han, Z.-H. (2009) Efficient uncertainty quantification using gradient-enhanced kriging. *11th AIAA Non-Deterministic Approaches Conference*, 2009-2276, 1–23. AIAA, Palm Springs, CA.
- Fekete, S., Diederichs, M. and Lato, M. (2010) Geotechnical and operational applications for 3-dimensional laser scanning in drill and blast tunnels. *Tunnelling and Underground Space Technology*, **25**, 614–628.
- Fuller, W.A. (2009) *Measurement Error Models*, John Wiley & Sons, Hoboken, NJ.
- Goldberg, P.W., Williams, C.K. and Bishop, C.M. (1997) Regression with input-dependent noise: A Gaussian process treatment. *Advances in Neural Information Processing Systems*, **10**, 493–499.
- Han, J.-Y., Guo, J. and Jiang, Y.-S. (2013) Monitoring tunnel deformations by means of multi-epoch dispersed 3D LiDAR point clouds: An improved approach. *Tunnelling and Underground Space Technology*, **38**, 385–389.
- Huang, D., Allen, T.T., Notz, W.I. and Zeng, N. (2006) Global optimization of stochastic black-box systems via sequential kriging meta-models. *Journal of Global Optimization*, **34**, 441–466.
- Huwig, L. and Huang, Y.S. (2000) On errors-in-variables in polynomial regression-Berkson case. *Statistica Sinica*, **10**, 923–936.
- Jin, R., Chang, C.-J. and Shi, J. (2012) Sequential measurement strategy for wafer geometric profile estimation. *IIE Transactions*, **44**, 1–12.
- Kersting, K., Plagemann, C., Pfaff, P. and Burgard, W. (2007) Most likely heteroscedastic Gaussian process regression, in *Proceedings of the 24th International Conference on Machine Learning*, ACM, Corvallis, OR, pp. 393–400.
- Li, D., Li, X.X., Li, Y.S. and Luo, Z.F. (2011) Analysis of temporal-spatial effect for tunnel construction in the fault-rupture zone. *Applied Mechanics and Materials*, **90**, 1981–1986.
- Lockwood, B.A. and Anitescu, M. (2012) Gradient-enhanced universal kriging for uncertainty propagation. *Nuclear Science and Engineering*, **170**, 168–195.
- MacKay, D.J. (1998) Introduction to Gaussian processes. *NATO ASI Series F Computer and Systems Sciences*, **168**, 133–166.
- Marshall, G.F. and Stutz, G.E. (2011) *Handbook of Optical and Laser Scanning*, CRC Press, Boca Raton, FL.
- Monserat, O. and Crosetto, M. (2008) Deformation measurement using terrestrial laser scanning data and least squares 3D surface matching. *ISPRS Journal of Photogrammetry and Remote Sensing*, **63**, 142–154.
- Näther, W. and Šimák, J. (2003) Effective observation of random processes using derivatives. *Metrika*, **58**, 71–84.
- Plumlee, M., Jin, R., Roshan Joseph, V. and Shi, J. (2013) Gaussian process modeling for engineered surfaces with applications to Si wafer production. *Stat*, **2**, 159–170.

- Ramoni, M. and Anagnostou, G. (2011) The effect of consolidation on TBM shield loading in water-bearing squeezing ground. *Rock Mechanics and Rock Engineering*, **44**, 63–83.
- Rasmussen, C.E. and Williams, C.K.I. (2006) *Gaussian Processes for Machine Learning*, MIT Press, Boston, MA.
- Reshetnyuk, Y. (2006) *Investigation and Calibration of Pulsed Time-of-Flight Terrestrial Laser Scanners*, Department of Transport and Economics, Royal Institute of Technology, Stockholm, Sweden.
- Santner, T.J., Williams, B.J. and Notz, W. (2003) *The Design and Analysis of Computer Experiments*, Springer Science & Business Media, New York, NY.
- Stein, M.L. (2012) *Interpolation of Spatial Data: Some Theory for Kriging*, Springer Science & Business Media, New York, NY.
- Titsias, M.K. and Lázaro-gredilla, M. (2011) Variational heteroscedastic Gaussian process regression, in *Proceedings of the 28th International Conference on Machine Learning (ICML-11)*, ACM, Bellevue, WA, pp. 841–848.
- Ulaganathan, S., Couckuyt, I., Dhaene, T., Degroote, J. and Laermans, E. (2016) Performance study of gradient-enhanced kriging. *Engineering with Computers*, **32**, 15–34.
- Van Gosliga, R., Lindenberg, R. and Pfeifer, N. (2006) Deformation analysis of a bored tunnel by means of terrestrial laser scanning. *ISPRS Commission V Symposium Image Engineering and Vision Metrology*, 167–172, ISPRS, Dresden, Germany.
- Walton, G., Delaloye, D. and Diederichs, M.S. (2014) Development of an elliptical fitting algorithm to improve change detection capabilities with applications for deformation monitoring in circular tunnels and shafts. *Tunnelling and Underground Space Technology*, **43**, 336–349.
- Wang, A., Wang, K. and Tsung, F. (2014) Statistical surface monitoring by spatial-structure modeling. *Journal of Quality Technology*, **46**, 359–376.
- Wang, L. (2004) Estimation of nonlinear models with Berkson measurement errors. *Annals of Statistics*, **32**, 2559–2579.
- Xia, H., Ding, Y. and Wang, J. (2008) Gaussian process method for form error assessment using coordinate measurements. *IIE Transactions*, **40**, 931–946.
- Zhang, L., Wang, K. and Chen, N. (2016) Monitoring wafers' geometric quality using an additive Gaussian process model. *IIE Transactions*, **48**, 1–15.
- Zimmermann, R. (2013) On the maximum likelihood training of gradient-enhanced spatial Gaussian processes. *SIAM Journal on Scientific Computing*, **35**, A2554–A2574.

## Appendix

### A-I MLE for GP

Based on Equation (2), the the log-likelihood of  $\Theta$  given  $\rho$  is

$$\log p_{\Theta}(\rho) = \text{const} - \frac{1}{2} \log \Sigma_0 - \frac{1}{2} \log(\rho_0 - \mu \mathbf{1}_n - r(\mathbf{X}))^T (\Sigma_0 + \Lambda_0)^{-1} (\rho - \mu \mathbf{1}_n - r(\mathbf{X})), \quad (\text{A1})$$

where  $\mathbf{x} = [\varphi, \theta]$ ,  $\mathbf{X} = [\mathbf{x}_1, \dots, \mathbf{x}_N]$ , and  $r(\mathbf{X}) = [r(\mathbf{x}_1), \dots, r(\mathbf{x}_N)]$  is the designed profile as defined earlier, and  $\Lambda_0$  is a diagonal matrix containing the variances of measurement errors. For Algorithm 1,  $\rho = [M_1, \dots, M_n]$  and  $\Lambda_0 = \text{diag}(S_1^2/m_1, \dots, S_n^2/m_n)$ . However, direct optimization of Equation (A1) is easily trapped in local optima. To improve the optimization performance, we can reduce the parameters' dimension by maximizing the profile likelihood.

In particular, we note that given  $\sigma_f^2$  and  $\mathbf{L} \equiv [l_x, l_y, l_z]$ , the choice of  $\hat{\mu}(\sigma_f^2, \mathbf{L})$  that maximizes Equation (A1) can be analytically obtained as

$$\hat{\mu}(\sigma_f^2, \mathbf{L}) = \frac{\mathbf{1}_n^T (\Sigma_0 + \Lambda_0)^{-1} \rho}{\mathbf{1}_n^T (\Sigma_0 + \Lambda_0)^{-1} \mathbf{1}_n}. \quad (\text{A2})$$

Subsequently,  $\sigma_f^2$  and  $\mathbf{L}$  can be estimated by maximizing the profile-likelihood (up to a constant):

$$\log p_{\{\sigma_f^2, l_x, l_y, l_z\}}(\rho | \hat{\mu}) = -\frac{1}{2} \log(\Sigma_0 + \Lambda_0) - \frac{1}{2} \log \hat{\mathbf{e}}^T (\Sigma_0 + \Lambda_0)^{-1} \hat{\mathbf{e}}, \quad (\text{A3})$$

with  $\hat{\mathbf{e}} = \rho - \hat{\mu} \mathbf{1}_n - r(\mathbf{X})$ . Numerical optimization methods can be used to solve Equation (A3) simultaneously. This optimization can be easier and more numerically stable since we separate the parameter set  $\Theta$  into two smaller sets. We minimize Equation (A3) using `SCIPY.OPTIMIZE` module in Python.

### A-II MLE for gradient-enhanced GP

For the augmented data, we have

$$\hat{\rho}_A | \Theta \sim \mathcal{N}(\mu \mathbf{1}_n^A + r_A(\mathbf{X}), \Sigma_A + \Lambda_A),$$

with  $\Theta = \{\mu, \sigma_f^2, l_x, l_y, l_z\}$ . Then the log-likelihood of  $\Theta$  is

$$\log p_{\Theta}(\hat{\rho}_A) = \text{const} - \frac{1}{2} \log \Sigma_A - \frac{1}{2} \log(\hat{\rho}_A - \mu \mathbf{1}_n^A - r_A(\mathbf{X}))^T (\Sigma_A + \Lambda_A)^{-1} (\hat{\rho}_A - \mu \mathbf{1}_n^A - r_A(\mathbf{X})). \quad (\text{A4})$$

Following the same idea as Appendix A-I, we have

$$\hat{\mu}(\sigma_f^2, \mathbf{L}) = \frac{\mathbf{1}_n^{AT} (\Sigma_A + \Lambda_A)^{-1} \hat{\rho}_A}{\mathbf{1}_n^{AT} (\Sigma_A + \Lambda_A)^{-1} \mathbf{1}_n^A} \quad (\text{A5})$$

and

$$\log p_{\{\sigma_f^2, l_x, l_y, l_z\}}(\hat{\rho}_A | \hat{\mu}) = -\frac{1}{2} \log(\Sigma_A + \Lambda_A) - \frac{1}{2} \log \hat{\mathbf{e}}^T (\Sigma_A + \Lambda_A)^{-1} \hat{\mathbf{e}}, \quad (\text{A6})$$

with  $\hat{\mathbf{e}} = \hat{\rho}_A - \hat{\mu} \mathbf{1}_n^A - r_A(\mathbf{X})$ . We solve it in the same way as Equation (A3).

### A-III Expression of unbiased correction constant

The sample standard deviation  $S$  is a biased estimation of  $\sigma$  with the fact that  $E[S] = c_4 \sigma$ . To derive the unbiased correction constant  $c_4$ , we assume the random variable  $X \sim \mathcal{N}(\mu, \sigma^2)$ , then  $S^2(n-1)/\sigma^2 \sim \chi_{n-1}^2$ . Let  $Z$  be distributed as  $\chi_{n-1}^2$ ; hence

$$\begin{aligned} \mathbb{E}[S] &= \sigma \mathbb{E}[Z^{1/2}]/(n-1)^{1/2} \\ &= \sigma [2/(n-1)]^{1/2} \Gamma(n/2)/\Gamma[(n-1)/2] \\ &= c_4 \sigma, \end{aligned}$$

where  $c_4 = [2/(n-1)]^{1/2} \Gamma(n/2)/\Gamma[(n-1)/2]$ . In addition, we can obtain

$$\begin{aligned} \mathbb{V}[S] &= \mathbb{E}[S^2] - (\mathbb{E}[S])^2 \\ &= \sigma^2 (1 - c_4^2). \end{aligned}$$